J. Phys.: Condens. Matter **11** (1999) 8591–8606. Printed in the UK PII: S0953-8984(99)03754-6

Magnetism in heavy-fermion U(Pt,Pd)$_3$ studied by μSR

R J Keizer†, A de Visser†‖, A A Menovsky†, J J M Franse†, A Amato‡, F N Gygax§, M Pinkpank§ and A Schenck§

† Van der Waals–Zeeman Institute, University of Amsterdam, Valckenierstraat 65, 1018 XE Amsterdam, The Netherlands
‡ Paul Scherrer Institute, CH-5232 Villigen, Switzerland
§ Institute for Particle Physics, ETH Zürich, PSI, CH-5232 Villigen, Switzerland

E-mail: devisser@wins.uva.nl

Received 22 April 1999, in final form 31 August 1999

Abstract. We report μSR experiments carried out on a series of heavy-electron pseudobinary compounds U(Pt$_{1-x}$Pd$_x$)$_3$ ($x \leqslant 0.05$). For $x \leqslant 0.005$ the zero-field muon depolarization is described by the Kubo–Toyabe function. However the temperature variation of the Kubo–Toyabe relaxation rate $\Delta_{KT}(T)$ does not show any sign of the small-moment antiferromagnetic phase with $T_N \approx 6$ K (signalled by neutron diffraction), in contrast to previous reports. The failure to detect the small ordered moment suggests it has a fluctuating (>10 MHz) nature, which is consistent with the interpretation of NMR data. For $0.01 \leqslant x \leqslant 0.05$ the muon depolarization in the ordered state is described by two terms of equal amplitude: an exponentially damped spontaneous oscillation and a Lorentzian Kubo–Toyabe function. These terms are associated with antiferromagnetic order with substantial moments. The Knight shift measured in a magnetic field of 0.6 T on single-crystalline U(Pt$_{0.95}$Pd$_{0.05}$)$_3$ in the paramagnetic state shows two signals for $\boldsymbol{B} \perp \boldsymbol{c}$, while only one signal is observed for $\boldsymbol{B} \parallel \boldsymbol{c}$. The observation of two signals for $\boldsymbol{B} \perp \boldsymbol{c}$, while there is only one muon localization site (0, 0, 0), points to the presence of two spatially distinct regions of different magnetic response.

1. Introduction

The heavy-fermion material UPt$_3$ continues to attract a great deal of attention, because of its unconventional magnetic and superconducting properties. The low-temperature normal state of UPt$_3$ [1, 2] presents an exemplary strongly renormalized Fermi liquid, with a quasiparticle mass of the order of 200 times the free electron mass, as evidenced by the large coefficient of the linear term in the specific heat, $\gamma = 0.42$ J mol^{-1} K^{-2}, and the equally enhanced Pauli susceptibility, $\chi_0(T \rightarrow 0)$. The magnetic properties of this hexagonal material are quite intriguing. The magnetic susceptibility $\chi(T)$ has a broad maximum at $T_{max} \approx 18$ K for a field in the hexagonal plane ($B \rightarrow 0$), which is attributed to the stabilization of antiferromagnetic interactions below T_{max}. For $T < T_{max}$ the magnetization $\sigma(B)$ exhibits a magnetic transition at a field $B^* = 20$ T ($\boldsymbol{B} \perp \boldsymbol{c}$). This continuous phase transition has been termed pseudo-metamagnetic and is interpreted as a suppression of the antiferromagnetic interactions. The most striking magnetic property of UPt$_3$ is undoubtedly the small-moment antiferromagnetic order (SMAF) which develops below the Néel temperature $T_N \approx 6$ K [3]. The ordered moment $m = 0.02\ \mu_B$/U atom is unusually small and is directed along the a^* axis in the hexagonal plane. The magnetic unit cell consists of a doubling of the nuclear unit cell along the a^* axis.

‖ Corresponding author: Dr A de Visser.

0953-8984/99/438591+16$30.00

This weak magnetic order has been documented extensively by neutron diffraction [3–7] and to a lesser extent by magnetic x-ray scattering [8]. It has not been observed reliably in the standard thermal, magnetic and transport properties, even by employing sensitive measuring techniques. Neutron-diffraction experiments [3] have demonstrated that SMAF and superconductivity ($T_c \sim 0.5$ K) coexist.

Substitution studies have demonstrated that UPt_3 is close to an antiferromagnetic instability [2, 9]. By replacing Pt by isoelectronic Pd pronounced phase transition anomalies appear in the thermal and transport properties. Notably, the λ-like anomaly in the specific heat and the chromium-type anomaly in the electrical resistivity give evidence for an antiferromagnetic phase transition of the spin-density-wave type. At optimal doping (5 at.% Pd) $T_{N,max} = 5.8$ K and the ordered moment equals $0.6 \pm 0.2\ \mu_B/U$ atom [7, 10]. In order to distinguish this phase from the SMAF of pure UPt_3 we have termed it the large-moment antiferromagnetic (LMAF) phase. The magnetic instability can also be triggered by substituting Th for U [11–13]. Remarkably, the magnetic phase diagrams for the (U, Th)Pt_3 and U(Pt, Pd)$_3$ pseudobinaries are almost identical. This shows that the localization of the uranium moments is not governed by the unit cell volume of these pseudobinaries (the unit cell volume decreases with Pd doping, while it increases with alloying with Th). Long-range magnetic order also shows up when UPt_3 is doped with 5 at.% Au, while substituting 5 at.% Ir, Rh, Y, Ce or Os does not induce magnetic order [14–16]. This indicates that a shape effect, i.e. the change in the c/a ratio, is the relevant control parameter for the occurrence of magnetic order.

The magnetic phase diagram of the $U(Pt_{1-x}Pd_x)_3$ series has been measured [7] by neutron diffraction and is shown in figure 1. The neutron-diffraction experiments have been performed on single-crystalline samples for $x \leqslant 0.05$ and the principal results are summarized as follows. The SMAF reported for pure UPt_3 is robust upon alloying and persists until at least $x = 0.005$. The ordered moment grows from $0.018 \pm 0.002\ \mu_B$/U atom for $x = 0$ to $0.048 \pm 0.008\ \mu_B$/U atom for $x = 0.005$. $T_N \approx 6$ K and, most remarkably, does not vary with Pd content. Near $x = 0.01$ the LMAF emerges. The ordered moment of this phase grows rapidly with Pd content and attains a maximum value of $0.63 \pm 0.05\ \mu_B$/U atom for $x = 0.05$ where also $T_N = 5.8$ K is a maximum. $T_N(x)$ for the LMAF follows a Doniach-type phase diagram [17]. From this diagram it has been inferred that the antiferromagnetic instability for the LMAF in $U(Pt_{1-x}Pd_x)_3$ is located in the range 0.5–1 at.% Pd. It is important to notice that the neutron-diffraction data are consistent with a single-q magnetic structure which is identical for both the SMAF and LMAF phases. However a triple-q structure for the SMAF phase cannot be excluded [6, 7].

In this paper we report a μSR study of the evolution of magnetism in U(Pt, Pd)$_3$. This work was carried out in parallel with the neutron-diffraction study [7]. Our main objectives were: (i) to investigate the evolution of the weak magnetic order as a function of Pd content, and (ii) to investigate the connection (or possible coexistence) between the SMAF and LMAF. The motivation of using the μSR technique stems from the extreme sensitivity to magnetic signals. Besides the muon acts as a local probe, which permits us to discern magnetically inequivalent sample regions. For recent reviews of μSR experiments on heavy-electron systems and magnetic materials we refer to [18] and [19].

Our work was in part inspired by the early μSR experiments on polycrystalline $(U_{1-x}Th_x)Pt_3$ reported by Heffner *et al* [20]. For undoped UPt_3 these authors observed small increases of the Kubo–Toyabe relaxation rate, Δ_{KT}, and the transverse-field Gaussian relaxation rate, σ_G, below ≈6 K. These increases were attributed to weak static magnetism with a magnetic moment of the order of 10^{-3}–$10^{-2}\ \mu_B$/U atom. This discovery in fact preceded the detection of SMAF by neutron diffraction. For $U_{0.95}Th_{0.05}Pt_3$, which orders antiferromagnetically at

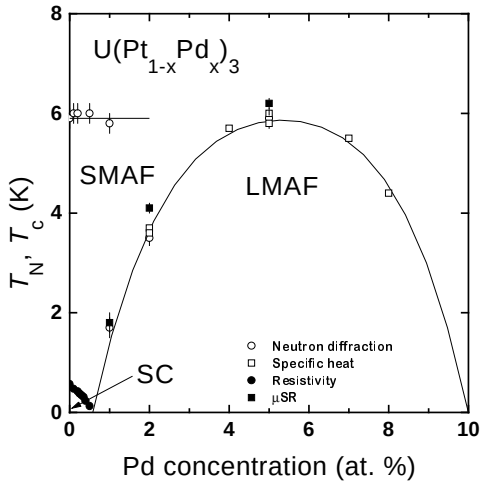

Figure 1. The Néel temperature, T_N, versus Pd concentration for $U(Pt_{1-x}Pd_x)_3$ alloys as determined from neutron diffraction (○), specific heat (□) and μSR (■) experiments. SMAF and LMAF denote small-moment and large-moment antiferromagnetic order, respectively. In the lower left corner the upper superconducting transition temperature as determined by resistivity experiments is given. SC denotes the superconducting phase. This neutron-diffraction and specific heat data are taken from [7].

$T_N = 6.2$ K with a large magnetic moment ($\approx 0.6\ \mu_B$/U atom), spontaneous μ^+ oscillations at frequencies of 2 and 8 MHz were detected below T_N, while for $U_{0.99}Th_{0.01}Pt_3$ no spontaneous oscillations were observed ($T > 4.2$ K).

In our μSR study we concentrate predominantly on the low-temperature magnetic properties of the doped compounds. One of the principal results is that we, quite unexpectedly, could not resolve the SMAF in the zero-field experiments carried out on polycrystalline $U(Pt_{1-x}Pd_x)_3$ with $x = 0$, 0.002 and 0.005. Also Dalmas de Réotier *et al* failed to detect the SMAF by μSR in their high-quality single-crystalline samples [21]. These results are at variance with the data reported in [20]. For higher Pd concentrations ($x = 0.01$, 0.02 and 0.05) we observe spontaneous μ^+ precession frequencies, similar to those reported for Th doped UPt_3 [20].

This paper is organized as follows. Section 2 is devoted to the experimental details, such as the sample preparation process, the characterization of the samples and some relevant parameters of the experimental set-up. In sections 3 and 4 we present the results of the zero-field (ZF) and low transverse field (TF $= 0.01$ T) measurements on the SMAF and LMAF states, respectively. In section 5 we present TF ($= 0.6$ T) experiments on single-crystalline $U(Pt_{0.95}Pd_{0.05})_3$. In section 6 we discuss our results, while the summary is presented in section 7. Parts of these results were presented in [22] and [23].

2. Experiment

The $U(Pt_{1-x}Pd_x)_3$ pseudobinaries crystallize in a hexagonal closed-packed structure ($MgCd_3$ type) with space group $P6_3/mmc$. The lattice parameters for $x = 0$ are given by $a = 5.764$ Å and $c = 4.899$ Å. The lattice parameter for the a axis for $x \leqslant 0.05$ is constant within the experimental accuracy, while the lattice parameter for the c axis decreases at a rate of 3×10^{-4} Å/at.% Pd. This results in a minute reduction of the c/a ratio.

We have prepared polycrystalline material with $x = 0.000$, 0.002, 0.005, 0.01, 0.02 and 0.05 by arc melting the constituents in a stoichiometric ratio in an arc furnace on a water-cooled copper crucible under a continuously Ti-gettered argon atmosphere (0.5 bar). Samples with low Pd contents ($x \leqslant 0.01$) were prepared by using appropriate master alloys (e.g. 5 at.% Pd). As starting materials we used natural uranium (JRC-EC, Geel) with a purity of 99.98%, and platinum and palladium (Johnson Matthey) with a purity of 99.999%. For annealing, the samples were wrapped in tantalum foil and put in water free quartz tubes together with a piece of uranium that served as a getter. After evacuating ($p < 10^{-6}$ mbar) and sealing the tubes, the samples were annealed at 950 °C for seven days. Next the samples were slowly cooled in three days to room temperature. For $x = 0.05$ a single-crystalline sample was pulled from the melt using a modified Czochralski technique in a tri-arc furnace under a continuously Ti-gettered argon atmosphere. The single-crystalline sample was annealed in a similar way as the polycrystalline material.

Four thin slices (thickness 0.8 mm, area 6×10 mm^2) were cut from the annealed polycrystalline buttons ($x = 0$, 0.002, 0.005, 0.01, 0.02 and 0.05) by means of spark erosion. The surface layer, defected by spark erosion, was removed by polishing with diamond paste (grain size 0.3 μm). The samples were glued on a silver support by General Electric varnish to cover the desired area for the μSR experiments: 12×20 mm^2. The single-crystalline sample ($x = 0.05$) was glued to a silver rod, which served as sample support.

Parts of the polycrystalline batches were characterized by electrical resistivity measurements. In agreement with the data presented in [24], the upper superconducting transition temperature T_c^+ amounts to 0.533 and 0.389 K, for $x = 0$ and 0.002, respectively. Also the residual resistivity, ρ_0, was found to increase linearly with Pd content ($x \leqslant 0.005$), which indicates that Pd dissolves homogeneously in the matrix. We obtain ρ_0 values of 0.88, 2.49, 6.2 and 12.0 $\mu\Omega$ cm for $x = 0.000$, 0.002, 0.005 and 0.01, respectively. For higher Pd concentrations ρ_0 rises more rapidly because of the spin-density-wave type of magnetic order. The Néel temperatures of the 2 and 5 at.% Pd polycrystalline sample determined by resistivity amount to 4.0 and 6.3 K, respectively. These values are slightly higher than measured previously on other batches (3.6 and 5.8 K) [2].

The μSR experiments were performed at the Paul Scherrer Institute (Villigen), using the μ^+SR-dedicated beam-line πM3. ZF and TF data were collected at the General Purpose Spectrometer (GPS) using a ^{4}He flow cryostat ($T > 1.6$ K). Here also the angular variation of the Knight shift was measured using an automated stepping motor device. Additional ZF and TF data were taken at the Low Temperature Facility (LTF), which is equipped with a top-loading ^{3}He–^{4}He dilution refrigerator (Oxford Instruments) with a base temperature of 0.025 K. By changing the operation mode of the dilution refrigerator temperatures up to ≈10 K can be reached.

3. μSR experiments on SMAF compounds ($x \leqslant 0.005$)

Zero-field μSR experiments have been performed on polycrystalline U(Pt$_{1-x}$Pd$_x$)$_3$ samples with $x = 0.000$ in the temperature (T) interval 2.7–7.0 K, with $x = 0.002$ in the T interval 0.9–8.0 K and with $x = 0.005$ in the T interval 0.03–10 K. Some typical muon depolarization curves, taken on the $x = 0.005$ compound at $T = 0.1$ K and 9.0 K, are shown in figure 2. For $x \leqslant 0.005$, the muon depolarization for $T < 10$ K is best described by the standard Kubo–Toyabe function:

$$G_{KT}(\Delta_{KT}t) = \tfrac{1}{3} + \tfrac{2}{3}(1 - \Delta_{KT}^2 t^2)\exp(-\tfrac{1}{2}\Delta_{KT}^2 t^2). \quad (1)$$

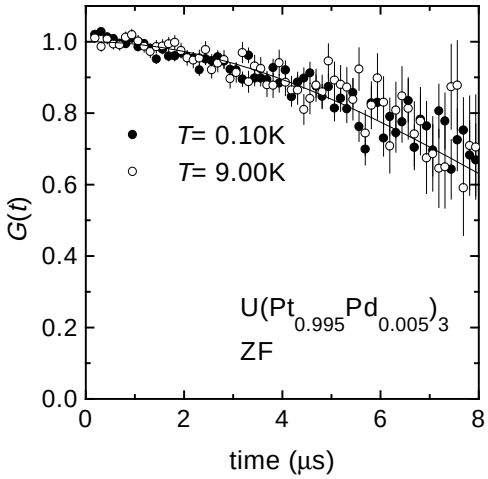

Figure 2. Typical zero-field spectra measured for polycrystalline $U(Pt_{0.995}Pd_{0.005})_3$. The solid line represents a fit to the Kubo–Toyabe function. The muon depolarization is the same above and below the antiferromagnetic transition ($T_N \approx 6$ K).

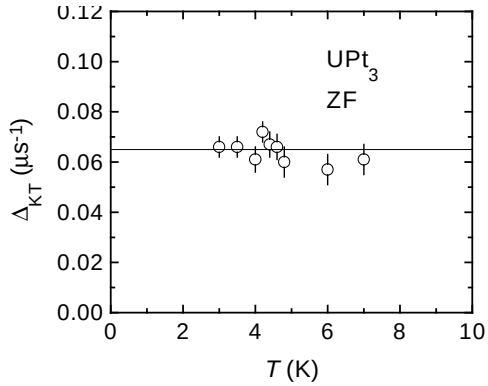

Figure 3. Zero-field Kubo–Toyabe line width, Δ_{KT}, for polycrystalline UPt_3. The solid line indicates the average value.

Here $\Delta_{KT} = \gamma_\mu \sqrt{\langle B^2 \rangle}$ is the Kubo–Toyabe relaxation rate, with γ_μ the muon gyromagnetic ratio ($\gamma_\mu/2\pi = 135.5$ MHz T^{-1}) and $\langle B^2 \rangle$ the second moment of the field distribution at the muon site. The Kubo–Toyabe function describes the case of an isotropic Gaussian distribution of static internal fields centred at zero field. The solid line in figure 2 presents a fit to the Kubo–Toyabe function for $x = 0.005$. In figures 3, 4 and 5 $\Delta_{KT}(T)$ is plotted for $x = 0.000$, 0.002 and 0.005, respectively. We conclude that Δ_{KT} shows no significant temperature dependence. The average values of Δ_{KT} are 0.065 ± 0.005, 0.058 ± 0.009 and $0.083 \pm 0.004\ \mu s^{-1}$ for $x = 0.000, 0.002$ and 0.005, respectively. Additional data for $x = 0.002$ were taken in a transverse field (perpendicular to the muon spin direction) of 0.010 T. Best fits were obtained using a Gaussian damped oscillation: $G(t) = \cos(2\pi\nu t + \phi)\exp(-1/2(\sigma_G t)^2)$. The Gaussian linewidth, σ_G, equals $0.081 \pm 0.007\ \mu s^{-1}$ and is temperature independent as well (see figure 4).

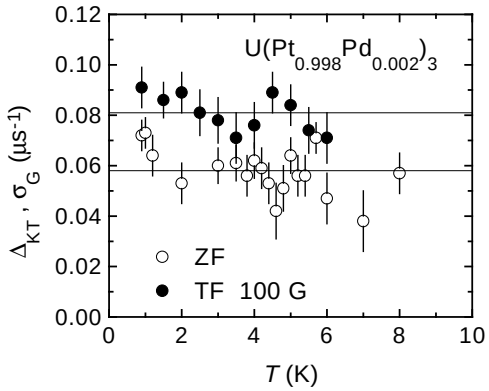

Figure 4. Zero-field Kubo–Toyabe line width (○) and transverse field (0.01 T) Gaussian line width (●) for polycrystalline $U(Pt_{0.998}Pd_{0.002})_3$. The solid lines indicate the average values.

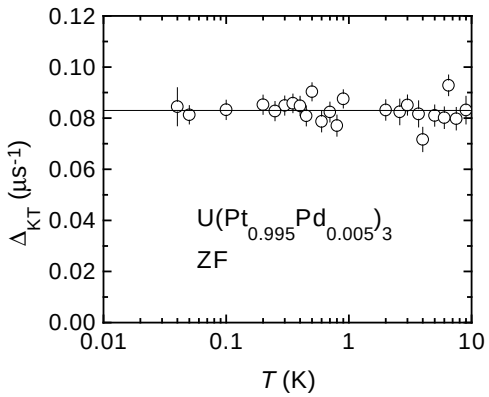

Figure 5. Zero-field Kubo–Toyabe line width for polycrystalline $U(Pt_{0.995}Pd_{0.005})_3$. The solid line indicates the average value.

Surprisingly, our data for polycrystalline UPt_3 are at variance with the results reported by Heffner *et al* [20] who observed a doubling of Δ_{KT}, from 0.06 μs^{-1} just above 6 K to 0.12 μs^{-1} in the limit $T \rightarrow 0$ K. As the doubling of Δ_{KT} was attributed to the presence of weak magnetic order (according to neutron diffraction SMAF), we conclude that the weak magnetic order does not show up in the ZF μSR signals for $x \leqslant 0.005$. It does also not show up in the TF $= 0.010$ T data. At this point it is important to realize that the neutron-diffraction experiments [7] show that for $x \leqslant 0.005$ SMAF invariably sets in at $T_N \approx 6$ K, while the ordered moment grows with Pd content: $m = 0.018 \pm 0.002$ μ_B/U atom, 0.024 ± 0.003 μ_B/U atom and 0.048 ± 0.008 μ_B/U atom for $x = 0.000$, 0.002 and 0.005, respectively. One could argue that the occurrence of SMAF is related to the single-crystalline nature of the samples used for neutron diffraction. However, the single- and polycrystalline samples were prepared using the same high-purity starting materials and also the ρ_0 values are about the same. Our unexpected result is in agreement with recent experiments on high-purity single-crystalline UPt_3 carried out by Dalmas de Réotier *et al* [19, 21]. These authors did not detect SMAF in their ZF μSR data, while neutron-diffraction measurements carried out on parts of the samples show that SMAF is present with the usual characteristics. Two explanations for the absence of SMAF in the μSR signals are conceivable: (i) the muons stop at sites where the dipolar fields due to

the SMAF and the direct contact field cancel, and (ii) the antiferromagnetic moment fluctuates at a rate >10 MHz, i.e. too fast to be detected by μSR, but slower than the time scale of the neutron-diffraction experiment ≈0.1 THz. We come back to this most important issue in section 6.

The zero-field data for $x \leqslant 0.005$ (figures 3–5) can be attributed entirely to the depolarization of the muon due to static ^{195}Pt nuclear moments. For pure UPt_3 and $U(Pt_{0.998}Pd_{0.002})_3$ experiments in a small (0.010 T) longitudinal field (along the muon spin direction) confirmed the static origin. We have calculated Δ_{KT}^2 due to nuclear moments using the expression [25, 26]:

$$\Delta_{KT}^2 = \frac{1}{6}\sum_j I_{Pt}(I_{Pt}+1)\left(\frac{\mu_0}{4\pi}\gamma_\mu\gamma_{Pt}\hbar\right)^2\frac{5-3\cos^2(\theta_j)}{r_j^6}. \qquad (2)$$

Here the sum is over all ^{195}Pt nuclei (abundance 33.7%) with spin $I_{Pt} = 1/2$ and gyromagnetic ratio γ_{Pt} ($\gamma_{Pt}/2\pi = 8.781$ MHz T^{-1}), which are located at a distance r_j from the muon localization site at an angle θ_j with respect to the muon spin (μ_0 is the permeability of free space). For the most probable muon localization sites the calculated values of Δ_{KT} range between 0.05 and 0.08 μs^{-1} (see table 1). These calculations were performed for pure UPt_3, but for small amounts of Pt substituted by Pd, which has no nuclear moment, the corrections can be neglected. Since the measured values of Δ_{KT} also fall in the range 0.05–0.08 μs^{-1} one cannot determine the stopping site from the depolarization due to the nuclear moments.

Table 1. The calculated Kubo–Toyabe line widths, Δ_{KT}, of UPt_3 in the polycrystalline limit for axial symmetric sites. The first column gives the multiplicity and the Wyckoff letter of the particular site. The numbers between parentheses denote the error in averaging over the possible ^{195}Pt configurations around the muon using the Monte Carlo method.

	Site	Δ_{KT} (μs^{-1})
2a	0 0 0	0.061(1)
2b	0 0 1/4	0.081(1)
4e	0 0 1/8	0.073(1)
4f	2/3 1/3 0	0.046(1)
2d	2/3 1/3 1/4	0.079(1)

4. LMAF probed by μSR experiments for $x \geqslant 0.01$

Zero-field μSR experiments have been performed on polycrystalline $U(Pt_{1-x}Pd_x)_3$ samples with $x = 0.01$ in the T interval 0.03–3 K, with $x = 0.02$ in the T interval 1.6–8.0 K and with $x = 0.05$ in the T interval 3.0–10 K. Additional experiments on a single-crystalline $x = 0.05$ sample confirm the results obtained on the polycrystal. For all samples we can identify a magnetic phase transition temperature, where below a spontaneous μ^+ precession frequency appears. This phase transition, which takes place at 1.8, 4.1 and 6.2 K for $x = 0.01$, 0.02 and 0.05, respectively, is to the LMAF state. This is confirmed by the neutron-diffraction study on single-crystalline $U(Pt_{1-x}Pd_x)_3$, from which it follows that the Néel temperature equals 1.8, 3.5 and 6.2 K, and the ordered moment equals 0.11 ± 0.03, 0.35 ± 0.05 and 0.63 ± 0.05 μ_B/U atom, for $x = 0.01$, 0.02 and 0.05, respectively [7].

Since the magnetic behaviour does not vary strongly for $0.01 \leqslant x \leqslant 0.05$, we have fitted the μSR spectra of the three LMAF compounds with one and the same expression. Previously we have fitted the data of the $x = 0.05$ compound with two spontaneous frequency components [22], while the data for $x = 0.01$ have been analysed using one spontaneous

frequency component and one exponential damping term [23]. The analysis with two terms, namely a standard depolarization function for a polycrystalline magnet, $G_\nu(t)$, and a Lorentzian Kubo–Toyabe function, $G_{\mathrm{KL}}(\lambda_{\mathrm{KL}}t)$, yields a more consistent description when all Pd concentrations ($x = 0.01, 0.02, 0.05$) are considered. Below T_{N} good fits are obtained using the following depolarization function:

$$G(t) = A_1 G_\nu(t) + A_2 G_{\mathrm{KL}}(\lambda_{\mathrm{KL}}t) \tag{3}$$

where

$$G_\nu(t) = \tfrac{2}{3}\exp(-\lambda t)\cos(2\pi\nu t + \phi) + \tfrac{1}{3}\exp(-\lambda' t) \tag{4a}$$

$$G_{\mathrm{KL}}(\lambda_{\mathrm{KL}}t) = \tfrac{1}{3} + \tfrac{2}{3}(1 - \lambda_{\mathrm{KL}}t)\exp(-\lambda_{\mathrm{KL}}t). \tag{4b}$$

The Lorentzian Kubo–Toyabe term (equation (4*b*)) represents an isotropic Lorentzian distribution of internal fields with an average zero field. At the moment we do not have a satisfactory explanation why the most consistent analysis requires the Lorentzian Kubo–Toyabe term. It implies that the spectral distribution of the internal fields is better approximated by a Lorentzian rather than a Gaussian field distribution. In this respect the use of equation (3) may be considered as a phenomenological approach. Consequently, the deduced parameters are phenomenological. Equation (3) assumes two magnetically different muon stopping sites. Note that two magnetic sites do not necessarily require two crystallographically different sites.

In the paramagnetic state ($T > T_{\mathrm{N}}$) the muon depolarization is best described by the standard Kubo–Toyabe function $G_{\mathrm{KT}}(\Delta_{\mathrm{KT}}t)$ (equation (1)), just as for the SMAF compounds ($x \leqslant 0.005$), with values of Δ_{KT} comparable to the values reported in figures 3–5. For $T \ll T_{\mathrm{N}}$ we find $A_1 = A_2$. This suggests that half of the muons stop at sites where the dipolar fields cancel, while the other half stop at sites with a net local dipolar magnetic field.

In order to show that equation (3) accounts for the LMAF state we have plotted in figures 6 and 7 the spontaneous frequency $\nu(T)$ and the depolarization rate of the Lorentzian Kubo–Toyabe function, $\lambda_{\mathrm{KL}}(T)$, respectively. For the LMAF state we found that the order parameter $m(T)$ as measured by neutron diffraction [7] could be described by $f(T) = f(0)(1 - (T/T_{\mathrm{N}})^{\alpha})^{\beta}$. The same expression, with almost identical values of α and β, yields a proper description of $\nu(T)$ and $\lambda_{\mathrm{KL}}(T)$ as well (see solid lines in figures 6 and 7). The fit parameters are listed in table 2. For $x = 0.02$ and 0.05 the values of β are close to the theoretical value $\beta = 0.38$ for the 3D Heisenberg model [27]. The phenomenological parameter α reflects spin-wave excitations. In a cubic antiferromagnetic system α is predicted to be 2 [28]. To our knowledge no predictions are available for a hexagonal system. A point of concern is that for a simple polycrystalline magnet one expects the spontaneous frequency $\nu(0)$ to scale with the ordered moment, which is clearly not the case here, as follows from the data in table 2. However, $\lambda_{\mathrm{KL}}(0)$ scales with the ordered moment. We comment on this point in the next paragraph.

In order to demonstrate the relative weight of the terms in equation (3) to the total depolarization function, we have plotted $G_\nu(t)$ and $G_{\mathrm{KL}}(\lambda_{\mathrm{KL}}t)$ in figure 8 for a typical μSR spectrum in the LMAF state, taken on $U(Pt_{0.99}Pd_{0.01})_3$ at $T = 0.1$ K. In figure 9 the concentration dependence of $G_\nu(t)$ and $G_{\mathrm{KL}}(\lambda_{\mathrm{KL}}t)$ is shown. Whereas $G_{\mathrm{KL}}(\lambda_{\mathrm{KL}}t)$ varies smoothly with Pd content, $G_\nu(t)$ is almost identical for $x = 0.02$ and 0.05. If both signals were to originate from the same ordered moment, then λ_{KT} and ν should both increase proportionally to the ordered moment. A possible reason for the absence of scaling of the frequency with the ordered moment is that the expression for $G_\nu(t)$ is only valid when $\lambda \ll \omega = 2\pi\nu$. Such a situation is described in [29] for a Gaussian field distribution. When λ is of the same order as ν large systematic errors can influence the fit parameters of $G_\nu(t)$. Since we deal with heavily damped spontaneous oscillations this is in part the case. The temperature dependence of λ is

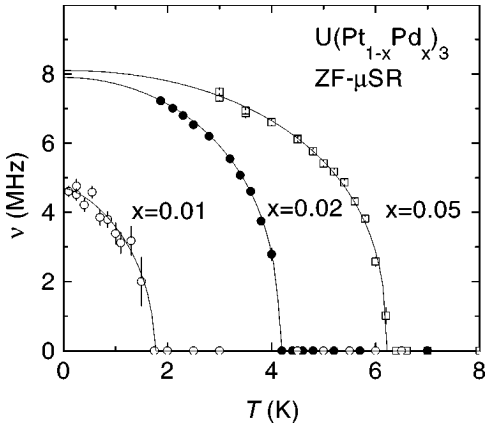

Figure 6. Temperature variation of the spontaneous frequency ν for polycrystalline $U(Pt_{1-x}Pd_x)_3$ with $x = 0.01$, 0.02 and 0.05 (see equation (3)). The solid lines represent fits to the function $f(T) = f(0)(1-(T/T_N)^{\alpha})^{\beta}$ (see text).

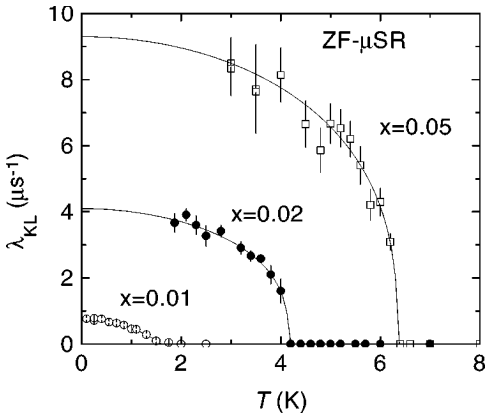

Figure 7. Temperature variation of λ_{KL} for polycrystalline $U(Pt_{1-x}Pd_x)_3$ with $x = 0.01$, 0.02 and 0.05 (see equation (3)). The solid lines represent fits to the function $f(T) = f(0)(1-(T/T_N)^{\alpha})^{\beta}$ (see text). $\lambda_{KL}(T)$ scales with the ordered moment.

plotted in figure 10, which shows that λ is almost constant below T_N for $x = 0.02$ and 0.05, with average values of 5.2 ± 0.5 and $6.1 \pm 0.5\ \mu s^{-1}$, respectively. The fit to equation (3) results in values $\lambda/\omega \approx 0.1$. Using the procedure as described in [29] we arrive at a correction of ν of only ≈10%. This small correction cannot explain the absence of scaling between ν and the ordered moment.

5. Transverse field μSR on $U(Pt_{0.95}Pd_{0.05})_3$

In an attempt to determine the muon localization site in the $U(Pt_{1-x}Pd_x)_3$ pseudobinaries we have carried out μSR experiments for $x = 0.05$ in transverse fields $B_{ext} = 0.6$ T in the temperature interval 10–250 K. The sample was shaped into a cube (dimensions $5 \times 5 \times 5\ mm^3$) with edges along the principal crystallographic directions. Let us first focus on the low-temperature data. In order to determine the frequency components in the spectra for $\boldsymbol{B}_{ext} \parallel \boldsymbol{a}$

Table 2. Fitting parameters for the LMAF state, determined from the zero-field temperature dependences of m, λ_{KL} and ν, described by the relation $f(T) = f(0)(1 - (T/T_N)^{\alpha})^{\beta}$. The subscript ND refers to parameters determined from neutron-diffraction experiments, while the subscripts KL and ν refer to the parameters determined from the μSR data (see equation (3)). The numbers between parentheses denote the error.

x	$m(0)$ (μ_B)	$T_{N,ND}$ (K)	α_{ND}	β_{ND}
0.01	0.11(3)	1.6(2)	—	—
0.02	0.34(5)	3.5(2)	1.9(2)	0.50(5)
0.05	0.63(5)	5.8(1)	1.8(1)	0.32(3)
	$\lambda_{KL}(0)$ (μs^{-1})	$T_{N,KL}$ (K)	α_{KL}	β_{KL}
0.01	0.76(5)	1.58(8)	1.9(4)	0.85(30)
0.02	4.1(3)	4.16(6)	1.9(2)	0.36(5)
0.05	9.3(9)	6.35(12)	2.0(5)	0.36(6)
	$\nu(0)$ (MHz)	$T_{N,\nu}$ (K)	α_{ν}	β_{ν}
0.01	4.7(2)	1.75(9)	1.5(4)	0.48(9)
0.02	7.9(1)	4.15(1)	2.0(2)	0.39(2)
0.05	8.1(1)	6.21(1)	2.1(3)	0.39(2)

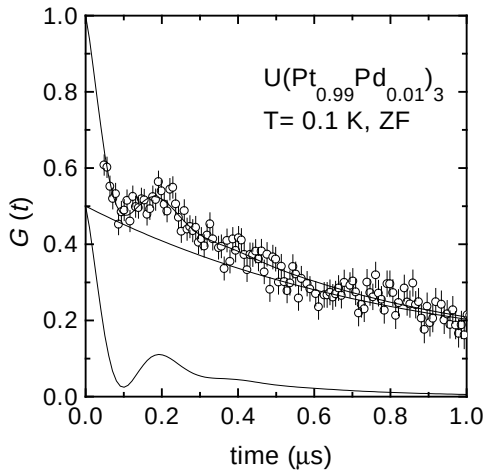

Figure 8. Typical zero-field spectrum measured for polycrystalline $U(Pt_{0.99}Pd_{0.01})_3$ at $T = 0.1$ K. The lines represent the different components of the fit (see equation (3)).

and $\boldsymbol{B}_{ext} \parallel \boldsymbol{c}$ at 10 K we have calculated the Fourier transforms, shown in figure 11. Inspecting the Fourier transforms we notice a remarkable difference for $\boldsymbol{B}_{ext} \parallel \boldsymbol{a}$ and $\boldsymbol{B}_{ext} \parallel \boldsymbol{c}$. Besides the background signal at 81.55 MHz, which is due to muons stopping in the silver sample support, we observe two signals for $\boldsymbol{B}_{ext} \parallel \boldsymbol{a}$ but only one signal for $\boldsymbol{B}_{ext} \parallel \boldsymbol{c}$. For $T > 10$ K, the two signals for $\boldsymbol{B}_{ext} \parallel \boldsymbol{a}$ are no longer observed in the Fourier transform. Instead, a single but always asymmetric peak is observed.

Therefore we have analysed the spectra for $\boldsymbol{B}_{ext} \parallel \boldsymbol{a}$ ($T = 10$–250 K) with the following three-component depolarization function, $G_a(t)$:

$$G_a(t) = A_1 \, e^{-\lambda_1 t} \cos(2\pi \nu_1 t + \varphi) + A_2 \, e^{-\lambda_2 t} \cos(2\pi \nu_2 t + \varphi) + A_{bg} \, e^{-\lambda_{bg} t} \cos(2\pi \nu_{bg} t + \varphi). \quad (5)$$

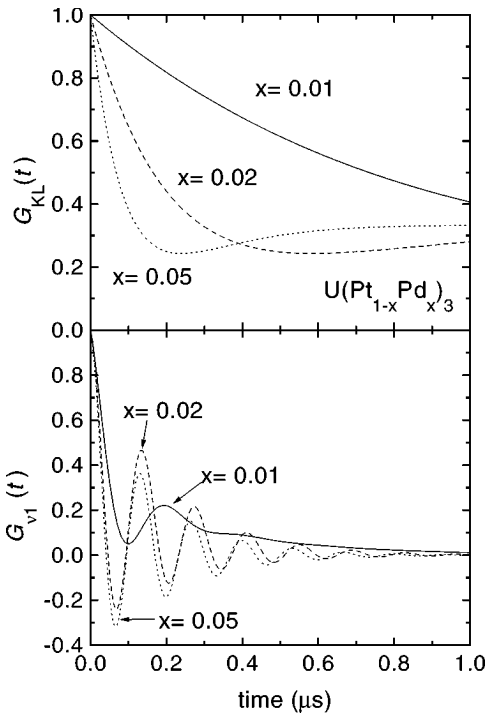

Figure 9. Contributions to the muon depolarization function (see equation (3)) in the ordered state for polycrystalline $U(Pt_{1-x}Pd_x)_3$ with $x = 0.01$, 0.02 and 0.05 at $T = 0.25$, 2 and 3 K, respectively. Upper frame: Lorentzian Kubo–Toyabe function. Lower frame: exponentially damped oscillating component.

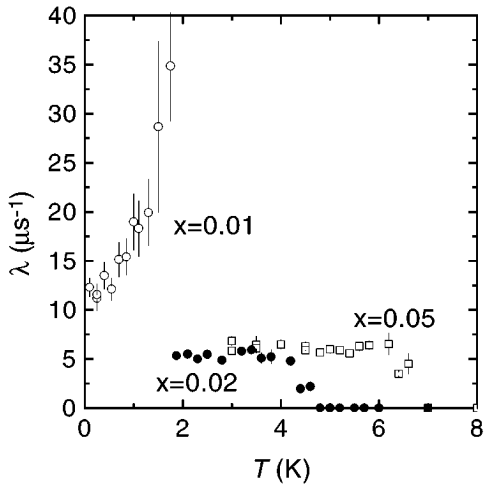

Figure 10. Temperature variation of the damping parameter λ of the oscillatory term for polycrystalline $U(Pt_{1-x}Pd_x)_3$ with $x = 0.01$, 0.02 and 0.05 (see equation (3)).

The first two components account for the μSR signal from the sample and the third component is the background signal. Although the first two signals are not resolved in the frequency domain for $T > 10$ K, it is possible to fit both components in the time domain by fixing

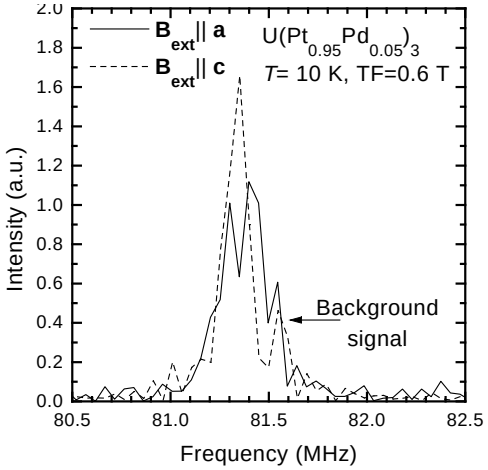

Figure 11. Fourier transforms of the spectra measured at 10 K in a transverse field of 0.6 T for single-crystalline $U(Pt_{0.95}Pd_{0.05})_3$: solid line $\boldsymbol{B} \parallel \boldsymbol{a}$, dotted line $\boldsymbol{B} \parallel \boldsymbol{c}$. The arrow indicates the background signal.

$A_1 = A_2$. In equation (5) the envelopes of the oscillating functions are exponentials. We also tried Gaussian damping, but it was not possible to discriminate between exponential or Gaussian damping terms. The resulting frequencies ν_1 and ν_2 are hardly influenced by the choice of the envelope function. For $\boldsymbol{B}_{\rm ext} \parallel \boldsymbol{c}$ we have analysed the spectra using the following two-component depolarization function, $G_c(t)$:

$$G_c(t) = A\,\mathrm{e}^{-\lambda t}\cos(2\pi\nu t + \varphi) + A_{\rm bg}\,\mathrm{e}^{-\lambda_{\rm bg} t}\cos(2\pi\nu_{\rm bg} t + \varphi). \tag{6}$$

From the measured frequencies we have determined the Knight shift $K = (B_{\rm loc}/B_{\rm ext}) - 1 = (\nu/\nu_0) - 1$, where $B_{\rm loc}$ is the field at the muon localization site and $\nu_0 = \gamma_\mu B_{\rm ext}/2\pi$. The Knight shift components for $\boldsymbol{B}_{\rm ext} \parallel \boldsymbol{a}$, $K_{a,\nu 1}(T)$ and $K_{a,\nu 2}(T)$, and for $\boldsymbol{B}_{\rm ext} \parallel \boldsymbol{c}$, $K_{c,\nu}(T)$, follow a Curie–Weiss behaviour in a limited T range only (50–100 K). For $T > 100$ K the difference, $\nu_1 - \nu_2$, between the two frequencies ($\boldsymbol{B}_{\rm ext} \parallel \boldsymbol{a}$) becomes smaller and above 150 K the data can only be fitted with one frequency. This indicates that slow muon hopping takes place for $T > 100$ K. As the muon diffuses, it experiences an average local magnetic field.

Next we compare the Knight shift with the susceptibility in order to determine the dipolar tensor components, A^{ii}. The susceptibility was measured on a different crystal using a SQUID magnetometer. For $T > 30$ K $\chi(T)$ follows a modified Curie–Weiss law, $\chi = \chi_0 + C/(T - \theta)$. The data are in excellent agreement with the results reported in [30]. In figure 12 we present K_i as a function of the bulk susceptibility, χ_i, in the so-called Clogston–Jaccarino plot, $K_i(\chi_i)$, where the temperature is an implicit parameter. Here $\boldsymbol{B} \parallel \boldsymbol{i}$, where $\boldsymbol{i}$ denotes the principal crystallographic directions. In general K_i scales with the susceptibility, $K_i = K_{\rm con} + A^{ii}\chi_i$. $K_{\rm con}$ is the Knight shift due to the direct contact field induced by the polarization by the conduction electrons. The Clogston–Jaccarino plot shows several remarkable features: (i) $K_a(\chi_a)$ deviates strongly from the expected linear behaviour, while $K_c(\chi_c)$ is approximately linear, and (ii) the direct contact contribution to the Knight shift ($T \to \infty$) $K_{\rm con}$ seems to be strongly anisotropic, while the unrenormalized Pauli susceptibility χ_0 is not. This strongly suggests that the local and bulk susceptibilities differ, which hampers the determination of the components of the dipolar tensor.

The angular variation of the Knight shift $K(\theta)$ measured on a spherical $U(Pt_{0.95}Pd_{0.05})_3$ sample [31] in the a–c plane follows a standard $\cos^2$ law, while $K(\theta)$ in the basal plane is

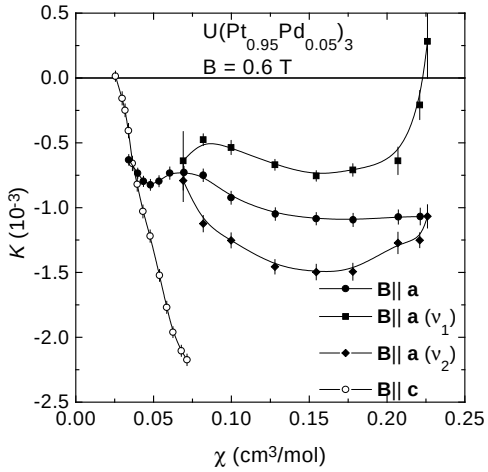

Figure 12. Clogston–Jaccarino plot for $U(Pt_{0.95}Pd_{0.05})_3$: (●) one-component fit for $\boldsymbol{B} \parallel \boldsymbol{a}$, (■,◆) two-component fit (ν_1, ν_2) for $\boldsymbol{B} \parallel \boldsymbol{a}$ and (○) $\boldsymbol{B} \parallel \boldsymbol{c}$. The temperature is an implicit parameter (10 K $< T <$ 250 K) with the low temperatures at the right side of the plot. The splitting for $\boldsymbol{B} \parallel \boldsymbol{a}$ disappears above 100 K.

isotropic. From this it follows that the muon localization site is restricted to axial symmetry. By analysing the $K(T)$ data in the temperature range 50–100 K with a modified Curie–Weiss type of expression, it has been concluded that there is only one stopping site, namely the 2a site, (0, 0, 0) [31]. The analysis of the Knight shift data taken on pure UPt_3 also points to the 2a site as the stopping site [32]. This shows that the muon localization site does not change at these small Pd concentrations.

The presence of two frequency components ($\boldsymbol{B} \parallel \boldsymbol{a}$) and only one stopping site provides strong evidence for two spatially distinct regions of different magnetic response up to at least ∼100 K. This is in line with a similar observation recently made for pure UPt_3 [33]. Whether the different magnetic response originates from macroscopically separated regions (e.g. domains) or is periodic in nature (e.g. a structural modulation [34]) remains an open problem.

6. Discussion

One of the unexpected conclusions from the present work is that SMAF ($x \leqslant 0.005$) is not detected in the zero-field μSR experiments. A first natural explanation of this result is that the SMAF is not present at all. However, this is contradicted by neutron-diffraction experiments. A simple calculation shows that the contribution to the dipolar field from the single-q (or possibly triple-q) magnetic structure cancels at the muon localization site (0, 0, 0). This offers a second explanation for not detecting the SMAF. Indeed, the measured values of Δ_{KT} (see section 3) are consistent with depolarization of the muon due to Pt nuclear moments only. Moreover, a comparison of the measured and calculated values of Δ_{KT} for axially symmetric stopping sites (table 1) is not inconsistent with the (0, 0, 0) stopping site. A third explanation for not observing the SMAF is that the antiferromagnetic moment fluctuates at a rate >10 MHz, i.e. too fast to be detected by μSR, but slower than the time scale of the neutron-diffraction experiment ≈0.1 THz. This explanation is particularly appealing because it also clarifies the absence of a signature of the SMAF in NMR experiments [35, 36]. Kohori *et al* [35] carried out ^{195}Pt NMR on the $U(Pt_{1-x}Pd_x)_3$ system. For compounds with LMAF (e.g. $x = 0.05$)

zero-field experiments showed that the transferred hyperfine field does not cancel at the Pt site. A simple calculation showed that the internal field originating from SMAF for $x = 0$ should have been observed as well; however, this turned out not to be the case. Since the symmetry argument for cancellation of the dipolar field does not hold for the Pt sites, the most probable explanation for the absence of the SMAF is the one of the fluctuating moment.

For $x \geqslant 0.01$ the LMAF is clearly observed in the zero-field μSR data. The muon depolarization in the ordered state is described by two terms of equal amplitude: an exponentially damped spontaneous oscillation and a Lorentzian Kubo–Toyabe function. However, it is not understood why the spontaneous frequency (ν) does not scale with the ordered moment, while the linewidth λ_{KL} does. Although the analysis of the Knight shift, measured in a transverse field of 0.6 T, shows that there is only one axial symmetric stopping site (0, 0, 0), we find two distinct values of K_{con} for $\boldsymbol{B} \parallel \boldsymbol{a}$ (see figure 12 and [31]). The observation of two contributions in the ordered state, i.e. one term with large spontaneous frequencies (in the range 4.7–8.1 MHz) and a second term described by the Lorentzian Kubo–Toyabe function, is possibly related to the large differences in K_{con}. At the moment we cannot offer an explanation how K_{con} and the spontaneous dipolar fields below T_N may be connected to each other, but the absence of scaling of the spontaneous frequency with the ordered moment m might be another indication for an unusual muon depolarization mechanism. High-resolution transverse-field experiments are needed to clarify these issues.

The μSR and neutron-diffraction studies demonstrate that SMAF and LMAF in the $U(Pt_{1-x}Pd_x)_3$ pseudobinaries are not closely connected. The differences between SMAF and LMAF are: (i) $T_N(x)$ attains a constant value of $\approx$6 K for SMAF, while $T_N(x)$ of the LMAF compounds follows a Doniach-type phase diagram, (ii) the squared order parameter $m^2(T)$ for the SMAF, as measured by neutron diffraction, grows in an unusual quasi-linear fashion, while the order parameter for the LMAF is conventional and confirms a real phase transition, and (iii) SMAF is not observed in zero-field μSR experiments in contrast to LMAF. The latter point we attribute to the fluctuating nature of the small ordered moment, which is consistent with NMR data [35, 36]. This strongly suggests that the SMAF does not present a true phase transition, but rather is a crossover phenomenon. The μSR and neutron-diffraction studies both show that LMAF is present for $x \geqslant 0.01$, while it is no longer observed for $x = 0.005$. This implies that the antiferromagnetic instability for the LMAF is located in the concentration range $x = 0.005$–0.01. μSR experiments on samples with intermediate Pd concentrations are under way in order to determine the critical concentration for LMAF, x_c. Of particular interest here is to investigate whether this critical concentration coincides with the critical concentration for the suppression of superconductivity $x_c = 0.007$ [24]. This would provide strong evidence that LMAF and superconductivity compete.

7. Summary

μSR experiments have been carried out on a series of pseudobinary polycrystalline heavy-electron $U(Pt_{1-x}Pd_x)_3$ compounds ($x \leqslant 0.05$). For $x \leqslant 0.005$ SMAF is not observed in the zero-field signals, whereas neutron diffraction shows that SMAF is stable upon alloying and $T_N(x) \approx 6$ K. The μSR spectra for $x \leqslant 0.005$ are consistent with depolarization of the muon due to nuclear moments only. The absence of SMAF signals in the ZF data is attributed to the fluctuating nature of the small ordered moment, consistent with NMR data [35, 36]. This strongly suggests that the SMAF does not present a true phase transition, but rather is a crossover phenomenon. For $0.01 \leqslant x \leqslant 0.05$ LMAF is clearly observed in the zero-field μSR data. The muon depolarization in the ordered state is described by two terms of equal amplitude: an exponentially damped spontaneous oscillation and a Lorentzian Kubo–Toyabe

function. The depolarization rate of the Lorentzian Kubo–Toyabe function, $\lambda_{KL}(T)$, was found to scale with the ordered moment $m(T)$ as measured by neutron diffraction. The Knight shift measured at 0.6 T on single-crystalline $U(Pt_{0.95}Pd_{0.05})_3$ in the paramagnetic state shows two signals for $\boldsymbol{B} \perp \boldsymbol{c}$, but only one signal for $\boldsymbol{B} \parallel \boldsymbol{c}$. In order to reconcile the observation of two signals for $\boldsymbol{B} \perp \boldsymbol{c}$ with the presence of only one stopping site $(0, 0, 0)$ [31], one has to evoke two spatially distinct regions of different magnetic response, as recently reported for pure UPt_3 [33].

Acknowledgments

We thank R van Harrevelt for contributing to this work in an early stage and C Baines for skilfully operating the LTF. A Yaouanc is gratefully acknowledged for stimulating discussions. This work was part of the research programme of the Dutch Foundation for Fundamental Research of Matter ('Stichting' FOM).

References

[1] Frings P H, Franse J J M, de Boer F R and Menovsky A 1983 *J. Magn. Magn. Mater.* **31–34** 240
[2] de Visser A, Menovsky A and Franse J J M 1987 *Physica* B **147** 81
[3] Aeppli G, Bucher E, Broholm C, Kjems J, Baumann J and Hufnagl J 1988 *Phys. Rev. Lett.* **60** 615
[4] Hayden S M, Taillefer L, Vettier C and Flouquet J 1992 *Phys. Rev.* B **46** 8675
[5] Lussier B, Taillefer L, Buyers W J L, Mason T E and Petersen T 1996 *Phys. Rev.* B **54** R6873
[6] van Dijk N H, Fåk B, Regnault L P, Huxley A and Fernández-Díaz M-T 1998 *Phys. Rev.* B **58** 3186
[7] Keizer R J, de Visser A, Menovsky A A, Franse J J M, Fåk B and Mignot J-M 1999 *Phys. Rev.* B **60** 6668
[8] Isaacs E D, Zschack P, Broholm C L, Burns C, Aeppli G, Ramirez A P, Palstra T T M, Erwin R W, Stücheli N and Bucher E 1995 *Phys. Rev. Lett.* **75** 1178
[9] de Visser A, Klaasse J C P, van Sprang M, Franse J J M, Menovsky A, Palstra T T M and Dirkmaat A J 1986 *Phys. Lett.* A **113** 489
[10] Frings P, Renker B and Vettier C 1987 *J. Magn. Magn. Mater.* **63/64** 202
[11] Ramirez A P, Batlogg B, Bucher E and Cooper A S 1985 *Phys. Rev. Lett.* **57** 1072
[12] Kadowaki K, Franse J J M and Woods S B 1987 *J. Magn. Magn. Mater.* **70** 403
[13] Goldman A I, Shirane G, Aeppli G, Batlogg B and Bucher E 1986 *Phys. Rev.* B **34** 6564
[14] Batlogg B, Bishop D J, Bucher E, Golding B Jr, Ramirez A P, Fisk Z and Smith J L 1987 *J. Magn. Magn. Mater.* **63/64** 441
[15] Kadowaki K, Klaasse J C P and Franse J J M 1988 *J. Magn. Magn. Mater.* **76/77** 233
[16] Kadowaki K, van Sprang M, Menovsky A A and Franse J J M 1987 *Japan. J. Appl. Phys.* **26** (Suppl. 26-3) 1243
[17] Doniach S 1977 *Physica* B **91** 231
[18] Amato A 1997 *Rev. Mod. Phys.* **69** 1119
[19] Dalmas de Réotier P and Yaouanc A 1997 *J. Phys.: Condens. Matter* **9** 9113
[20] Heffner R *et al* 1989 *Phys. Rev.* B **39** 11 345
[21] Dalmas de Réotier P, Huxley A, Yaouanc A, Flouquet J, Bonville P, Imbert P, Pari P, Gubbens P C M and Mulders A M 1995 *Phys. Lett.* A **205** 239
[22] de Visser A, Keizer R J, van Harrevelt R, Menovsky A A, Franse J J M, Amato A, Gygax F N, Pinkpank M and Schenck A 1997 *Physica* B **230–232** 53
[23] de Visser A, Keizer R J, van Harrevelt R, Menovsky A A, Franse J J M, Amato A, Gygax F N, Pinkpank M and Schenck A 1998 *J. Magn. Magn. Mater.* **177–181** 435
[24] Graf M J, Keizer R J, de Visser A and Franse J J M 1999 *Physica* B **259–261** 666
[25] Chappert J 1984 *Muons and Pions in Materials Research* ed J Chappert and R I Grynszpan (Amsterdam: Elsevier) ch 3
[26] Schenck A 1985 *Muon Spin Rotation Spectroscopy* (Bristol: Hilger)
[27] Domb C 1996 *The Critical Point* (London: Taylor and Francis)
[28] Kubo R 1952 *Phys. Rev.* **87** 568
[29] Kornilov E I and Pomjakushin V Yu 1991 *Phys. Lett.* A **153** 364
[30] van Sprang M, de Visser A, Franse J J M, Menovsky A and Dirkmaat A J 1987 *J. Magn. Magn. Mater.* **63/64** 393
[31] Schenck A *et al* 1999 *Physica* B at press (cond-mat/9909197)

[32] Schenck *et al*, to be published
[33] Yaouanc A *et al*, to be published
[34] Midgley P A, Hayden S M, Taillefer L, Bogenberger B and von Löhneysen H 1993 *Phys. Rev. Lett.* **70** 678
[35] Kohori Y, Kyogaku M, Kohara T, Asayama K, Amitsuka H and Miyako Y 1990 *J. Magn. Magn. Mater.* **90/91** 15
[36] Tou H, Kitaoka Y, Asayama K, Kimura N, Onuki Y, Yamamoto E and Maezawa K 1996 *Phys. Rev. Lett.* **77** 1374